FVTD Simulation for One Dimensional Rough Surface Scattering at Low-Grazing Angle

Kwang-yeol Yoon, Mitsuo Tateiba, Kazunori Uchida*
Department of Computer Science and Communication Engineering,
Kyushu University, 6-10-1, Hakozaki, Higashi-ku, Fukuoka, 812-8581,Japan
E-mail: yoon@green.csce.kyushu-u.ac.jp, tateiba@csce.kyushu-u.ac.jp
*Fukuoka Institute of Technology, 3-30-1, Wajiro-Higashi,
Higashi-ku, Fukuoka, 811-0295, Japan
E-mail: k-uchida@fit.ac.jp

1. INTRODUCTION

The electromagnetic wave scattering from a randomly rough surface has been widely studied because of its great importance in the fields of telecommunications and remote sensing. Reflection dominates in the high grazing limit. However, multiple scattering, shadowing and diffraction, which are difficult to model in theory, have strong effect on wave scattering in the low grazing limit. The widely used techniques for simulating the scattering properties from rough surfaces are small perturbation method (SPM), Kirchhoff Monte Carlo (KMC), integral equation (IE), and FDTD or FVTD [1 - 7]. The first SPM is limited only to the case where the average height of the rough surface is much smaller than the wavelength, and the second KMC ignores multiple scattering. The last IE and FVTD are numerical methods based on the wave theory. In this context, numerical methods are well suited to the rough surface problems in the case of low grazing angle (LGA). Unfortunately, numerical methods encounter difficulties in some cases. The incident wave propagates repeating multiple scattering along the rough surface at LGA. In order to simulate the scattering phenomenon accurately, we need a wide range of rough surface that is much larger than the wavelength. In a numerical sense, it corresponds to a large number of unknowns to be determined. Thus we need a powerful numerical method and much computer memory.

In this paper, we apply the FVTD method [8] to the wave scattering from dielectric one-dimensional (1-D) random rough surfaces at LGA. Numerical results are presented for the randomly rough surfaces of Gaussian type. First, we calculate the bistatic radar cross sections both for horizontal (hh) and vertical (vv) polarizations. Second, we compare the backscattering coefficient of the two different polarizations. Of particular interest is the ratio of backscattering between the horizontal and vertical polarizations, because it has been experimentally shown that the backscattering of vertical polarization is much larger than that of horizontal polarization at LGA [1]. The present results are compared with those obtained by IE and SPM [2]. In addition, we check the numerical convergence of FVTD by increasing the number of sampling points per wavelength. In our numerical simulations, we choose the sampling points per wavelength up to 80 in space domain. We also show some numerical results for the rough surface of length up to 1000 λ , where we choose 20 sampling points per wavelength in the space domain for the incidence angle between 5 and 10 degrees.

Numerical results demonstrate that the backscattering ratio of the two different polarizations is smaller than the predicted value based on the SPM. The present results are in agreement with the experimental data [1] and those based on the IE with 20 sampling points per wavelength. However, it should be noted that we need more sampling points per wavelength when a better accuracy is required.

2. FVTD FORMULATION

The geometry of problem is shown in Fig. 1. In FVTD formulation, the Maxwell equations are discretized on the basis of the volume integration with respect to a small cell. In the Cartesian coordinate system FVTD is equivalent to the conventional FDTD. However, FVTD is more effective to the inhomogeneous electromagnetic problems than FDTD, because FVTD employs averaged medium constants in each cell [8]. We consider an arbitrarily shaped boundary between two different electric and magnetic materials. One material is denoted by the constants with ε_{r1} =μ_{r1} =1.0 and σ_1 =0, and the other is designated by the constants (ε_{r2} ,μ_{r2} ,σ_2). We assume that one part of the (i,j)-th cell is occupied by the former material with area S_1 and the other part is occupied by the latter material with area S_2 as shown in Fig. 2. Then we can approximately evaluate the material constants in the (i,j)-th cell in an average fashion as follows:

$$\varepsilon'_{\mathbf{r}} = \frac{\varepsilon_{r1}\Delta S_1 + \varepsilon_{r2}\Delta S_2}{\Delta S}, \quad \mu'_{\mathbf{r}} = \frac{\mu_{r1}\Delta S_1 + \mu_{r2}\Delta S_2}{\Delta S}, \quad \sigma' = \frac{\sigma_1\Delta S_1 + \sigma_2\Delta S_2}{\Delta S} \tag{1}$$

where

$$\Delta S = \Delta S_1 + \Delta S_2 = \Delta x \Delta y \tag{2}$$

Now we summarize the FVTD formulations. For computational reason, magnetic field is normalized by the intrinsic impedance $Z_0 = \sqrt{\mu_0 / \varepsilon_0}$ as $\tilde{H} = Z_0 H$ where μ_0 and ε_0 are permeability and permittivity of the free space, respectively. Next we assign the averaged dielectric constant $\varepsilon_{ri,j}$, electric conductivity $\sigma_{i,j}$ in each cell. Then we

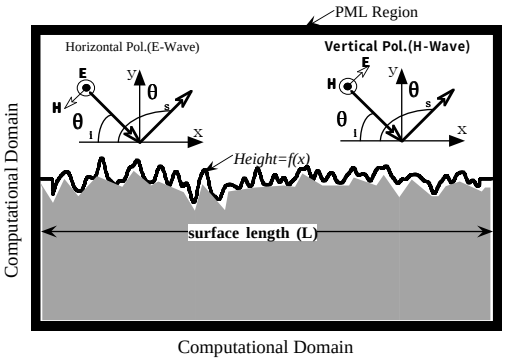

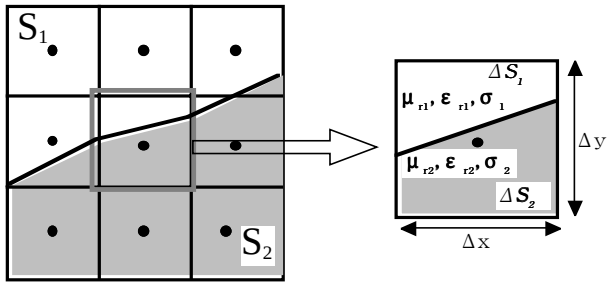

Fig. 1 Problem geometry including FVTD computation grid. **Fig. 2** Boundary value for arbitrary shaped surface.

can define the averaged and discretized electric field $E^n(i,j)$ in the (i,j)-th cell and in the n-th time point. Similarly we have the magnetic field $\tilde{H}^{n'}(i,j)$ in the n'-th time point where $n' = n - 1/2$. With these notations the FVTD equations for horizontal polarization are expressed as follows [8]:

$$\tilde{H}_x^{n'+1}(i,j) = \tilde{H}_x^{n'}(i,j) - \Gamma_y^{i,j} A^{i,j} Y_{i,j}[E_z^n(i,j+1) - E_z^n(i,j-1)] \tag{3}$$

$$\tilde{H}_y^{n'+1}(i,j) = \tilde{H}_y^{n'}(i,j) - \Gamma_x^{i,j} A^{i,j} Y_{i,j}[E_z^n(i+1,j) - E_z^n(i-1,j)] \tag{4}$$

$$\begin{aligned} E_z^{n+1}(i,j) = {} & \Omega^{i,j} E_z^n(i,j) - \Gamma_y^{i,j} B^{i,j} Z_{i,j}[\tilde{H}_x^{n'+1}(i,j+1) - \tilde{H}_x^{n'+1}(i,j-1)] \\ & + \Gamma_x^{i,j} B^{i,j} Z_{i,j}[\tilde{H}_y^{n'+1}(i+1,j) - \tilde{H}_y^{n'+1}(i-1,j)] \end{aligned} \tag{5}$$

The FVTD equations for the vertical polarization are expressed as follows [8]:

$$\tilde{H}_z^{n'+1}(i,j) = \tilde{H}_z^{n'}(i,j) - \Gamma_y^{i,j} Y_{i,j}[E_x^n(i,j+1) - E_x^n(i,j-1)] + \Gamma_x^{i,j} Y_{i,j}[E_y^n(i+1,j) - E_y^n(i-1,j)] \tag{6}$$

$$E_x^{n+1}(i,j) = \Omega^{i,j} E_x^n(i,j) + \Gamma_y^{i,j} B^{i,j} Z_{i,j}[\tilde{H}_z^{n'+1}(i,j+1) - \tilde{H}_z^{n'+1}(i,j-1)] \tag{7}$$

$$E_y^{n+1}(i,j) = \Omega^{i,j} E_y^n(i,j) + \Gamma_x^{i,j} B^{i,j} Z_{i,j}[\tilde{H}_z^{n'+1}(i+1,j) - \tilde{H}_z^{n'+1}(i-1,j)] \tag{8}$$

The step parameters used above are defined by

$$\begin{aligned} & \Gamma_{x,y}^{i,j} = \frac{c\Delta t}{2\sqrt{\varepsilon_{ri,j}}\Delta x,y}, \; A^{i,j} = \frac{1 - \exp(-\alpha_{mi,j})}{\alpha_{mi,j}}, \; Y_{i,j} = \frac{1}{Z_{i,j}} = \sqrt{\varepsilon_{ri,j}} \\ & B^{i,j} = \frac{1 - \exp(-\alpha_{i,j})}{\alpha_{i,j}}, \; \Omega^{i,j} = \exp(-\alpha_{i,j}), \; \alpha_{i,j} = \frac{\sigma_{i,j}\Delta t}{\varepsilon_0 \varepsilon_{ri,j}} \end{aligned} \tag{9}$$

where Δx and Δy are the space differences and Δt is the time difference. Moreover, $c = 1/\sqrt{\varepsilon_0 \mu_0}$ is the light velocity in the free space.

In the FVTD computation we have assumed the incident wave to be a modified Gaussian beam [3] as follows:

$$F^i(x,y) = \exp\{-j\vec{k}_{inc} \cdot r[1 + w(x,y)] - (x + y\cot\theta_i)^2 / g^2\} \tag{10}$$

where

$$w(x,y) = [2(x + y\cot\theta_i)^2 / g^2 - 1] / (kg\sin\theta_i)^2 \tag{11}$$

F is either the E_z or $\tilde{H}_z$ field, depending on the polarization considered. In (10) the θ_i is the incident angle measured from the horizontal, $\vec{k}_{inc} = k(\cos\theta\hat{x} + \sin\theta\hat{y})$, and $k = 2\pi/\lambda$, where λ is the free space electromagnetic wavelength. Moreover, the parameter g controls the tapering and the choice of g=L / 8 (except Fig. 3, g=L / 4) gives an acceptable tapering at the edges [2], where L is the finite surface length. We must pay much careful attention to the FVTD analysis when we treat a rough surface of long length compared with the wavelength because of the finite computer memory. We have used the PML absorbing boundary condition to reduce the end effect as small as possible [9].

3. SCATTERING FROM ROUGH SURFACE

FVTD allows us to compute near field data in the time domain just inside the PML region, and thus the near field data in the spectral domain are given by performing DFT. As a result, far field data can be calculated by the Kirchhoff-Huygense theorem. Let r and r' be the distances from the origin to the observation point (x,y) and to the equivalent source point (x',y'), and γ be the angle between these two distances.

$$r = \sqrt{x^2 + y^2}, \; r' = \sqrt{x'^2 + y'^2}, \; \cos\gamma = \frac{xx' + yy'}{rr'} \tag{12}$$

The Green's function is given by

$$G(r) = \frac{1}{4j} H_0^{(2)}(\kappa r) \tag{13}$$

where $H_0^{(2)}$ is the zero order Hankel function of the second kind, then the far fields can be calculated as follows:

$$\boldsymbol{D}_1 = \int_c (\boldsymbol{n} \times \tilde{\boldsymbol{H}})\, e^{jkr'\cos\gamma} ds \;\;,\;\; \boldsymbol{D}_{1m} = -\int_c (\boldsymbol{n} \times \boldsymbol{E})\, e^{jkr'\cos\gamma} ds \tag{14}$$

where $\boldsymbol{n}$ is the outward normal at the equivalent source point. With these relations, the scattered field in a far zone at a distance r from the center of the illuminated part of the surface can be found as

$$\tilde{\boldsymbol{H}}_z^s = -jk \frac{e^{-j\pi/4}}{2\sqrt{2\pi k}} \frac{e^{-jkr}}{\sqrt{r}} (\boldsymbol{u}_r \times \boldsymbol{D}) \;\;,\;\; \boldsymbol{E}_z^s = -jk \frac{e^{-j\pi/4}}{2\sqrt{2\pi k}} \frac{e^{-jkr}}{\sqrt{r}} \boldsymbol{D} \tag{15}$$

where $\tilde{\boldsymbol{H}}^s$ is for vertical polarization, or $\boldsymbol{E}^s$ is for horizontal polarization, and $\boldsymbol{D} = (\boldsymbol{u}_r \times \boldsymbol{D}_1 + \boldsymbol{D}_{1m}) \times \boldsymbol{u}_r$, where $\boldsymbol{u}_r$ is the unit vector in the r-direction.

The bistatic normalized radar cross section (NRCS) $\sigma^0(\theta_i,\theta_s)$ is defined by [4] as follows:

$$\sigma^0(\theta_i,\theta_s) = \lim_{r\to\infty} \frac{2\pi r \left| F^s \right|^2}{\int \left| F^i(x,0) \right|^2 dx} \tag{16}$$

where F^s is given by (15), and $F^s = \tilde{H}^s$ for vertical polarization, and $F^s = E^s$ for horizontal polarization. The backscattered NRCS is $\sigma^0(\theta_i,\theta_s) = \cos\theta_i\, \gamma^0(\theta_i,\theta_s)$. The scattering coefficient γ^0 is defined in terms of the projected area of the incident wave [10]:

$$\gamma^0(\theta_i,\theta_s) = \lim_{r\to\infty} \frac{2\pi r \left| F^s \right|^2}{\cos\theta_i \int \left| F^i(x,0) \right|^2 dx} \,. \tag{17}$$

Thus we have

$$\sigma^0(\theta_i,\theta_s) = \cos\theta_i\, \gamma^0(\theta_i,\theta_s) \,. \tag{18}$$

For the random rough surface the NRCS is averaged over an ensemble of finite surface realizations to obtain an ensemble average of NRCS $<\sigma^0(\theta_i,\theta_s)>$. According to the computational procedures described above, we can obtain the scattered far fields for two different polarizations, $\sigma^0_{(hh)}$ and $\sigma^0_{(vv)}$, for one rough surface profile. Then we can calculate the averaged backscatter cross sections of the horizontal and vertical polarizations as follows:

$$R_{(hh/vv)} = \frac{<\sigma^0_{(hh)}>}{<\sigma^0_{(vv)}>} \tag{19}$$

4. NUMERICAL RESULTS AND DISCUSSION

In this section, we present the numerical results of bistatic scattering and backscattering coefficients for different incidence angle as well as for different polarization. At L band (1.43GHz), the material constants are chosen as ε_{r2} =10.8, μ_{r2} =1.0 and σ_2 =0.106 (S/m) [2]. In this paper, we have assumed the Gaussian type of random rough surfaces with rms height as h=0.2 λ , and correlation length as cl=0.6 λ .

In Fig. 3, we check the numerical convergence by changing the number of sampling points per wavelength from 20 to 320, where the polarization is horizontal, and incident angle is selected as 10 and 45 degrees. This result indicates that more than 80 sampling points per wavelength should be used when accurate numerical results are needed. In Fig. 4, we demonstrate the numerical convergence with respect to surface length in case of horizontal polarization at the incident angle of 5 degrees. The surface length is selected as 200, 500, and 1000 λ for 50 randomly generated Gaussian surfaces. The two results of 500 and 1000 λ are in agreement except at forward scattering, but much difference is observed for 200 λ. As a result, it is necessary to select the surface length to be more than 500 λ at LGA.

In Fig. 5, we plot the backscattering coefficients both for horizontal and vertical polarizations at six incident angles between 5 and 10 degrees. The surface length is chosen as 500 λ and the IE results are also plotted (triangles) [2]. The two results are in good agreement when 20 sampling points per wavelength are chosen. To ensure numerical accuracy, we have also selected 80 sampling points per wavelength and observed much difference between 20 and 80 sampling points per wavelength. Unfortunately, the IE solution with 80 sampling points is not available at present.

Lastly, the ratio between horizontal and vertical backscattering is plotted in Fig. 6. It is demonstrated that 20 sampling points per wavelength is enough for calculating the ratio, even though the backscattering coefficients themselves are different from those calculated by using 80 sampling points as shown in Fig. 5. It is worth nothing that the SPM gives much larger ratio than the present numerical results.

5. CONCLUSIONS

In this paper, we have numerically analyzed the electromagnetic wave scattering from random rough surfaces by using FVTD method and then shown that the present method yields a reasonable solution even at LGA. The numerical results indicate that the vertical backscattering is larger than the horizontal one at LGA, and their ratio increases as the incident angle approaches near grazing. It should be noted that the number of sampling point per wavelength should be increased not only when more accurate numerical results are required but also when the relative permittivity is increased.

REFERENCES

[1] P. H. Y. Lee, J. D. Bater, K. L. Beach, C. L. Hindman, B. M. Lake, H. Rungaldier, J. C. Shelton, A. B. Williams, R. Yee, and H. C. Yuen, "X band microwave backscattering form ocean waves," *J. Geophysical Res*., vol. 100, No. C2, pp. 2591-2611, February 15, 1995.

[2] C. H. Chan, L. Tsang, Q. Li, "Monte Carlo simulations of large-scale one-dimensional random-rough surface scattering at near-grazing incidence: penetrable case," *IEEE Trans. Antennas Propagat.*, vol. 46, No. 1, pp. 142-149, Jan. 1998.

[3] E.I. Thoros, "The validity of the Kirchhoff approximation for rough surface scattering using a Gaussian roughness spectrum," *J. Acoust. Soc. Am.*, vol. 83, No. 1, pp. 78-92, January 1988.

[4] J. V. Toporkov, R. T. Marchand, G. S. Brown, "On the discretization of integral equation describing scattering by rough conducting surface," *IEEE Trans. Antennas Propagat.*, vol. 46, No. 1, pp. 150-161, January 1998.

[5] D. Holiday, L. L. DeRead, Jr., G. J. St-Cyr, "New equations for electromagnetic scattering by small perturbations of a perfectly conducting surface," *IEEE Trans. Antennas Propagat*., vol. 46, No.10, pp. 1427-1432, October 1998.

[6] F. D. Hastings, J. B. Schneider, S. L. Broschat, "A Monte-Carlo FDTD technique for rough surface scattering," *IEEE Trans. Antennas Propagat*., vol. 43, No. 11, pp. 1183-1191, November 1995.

[7] K. Y. Yoon, M. Tateiba, K. Uchida, "FVTD analysis of electromagnetic wave scattering from random or periodic structures," *KJJC-AP/ EMC/EMT'98*, pp 133-136, September 1998.

[8] K. Uchida, T. Matunaga, T. Noda and K.K. Han, "FVTD algorithm and its application procedure," *Res. Bull. Fukuoka Inst. Tech.*, vol.29, No. 1, pp. 121-130, Oct. 1996.

[9] J.P. Berenger, "A perfectly matched layer for the absorption of electromagnetic waves," *J.Comp. Phys.*, vol. 114, No. 2, pp. 185-200, October 1994.

[10] A. Ishimaru, Electromagnetic Wave Propagation, Radiation, and Scattering (Prentice-Hall, Inc. 1991).

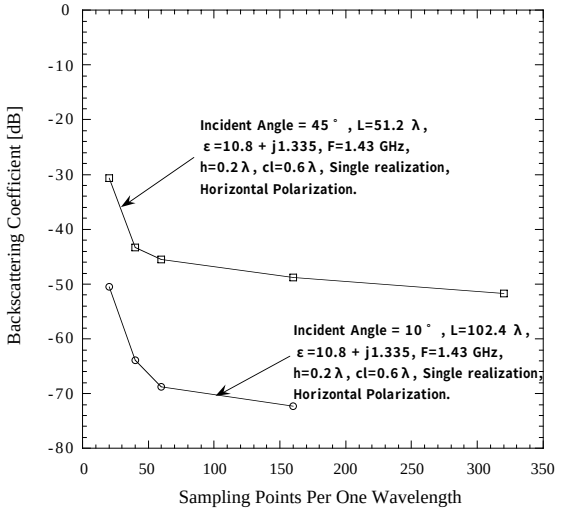

Fig. 3 Comparison of the variation of backscattering coefficients with respect to the number of sampling points per wavelength.

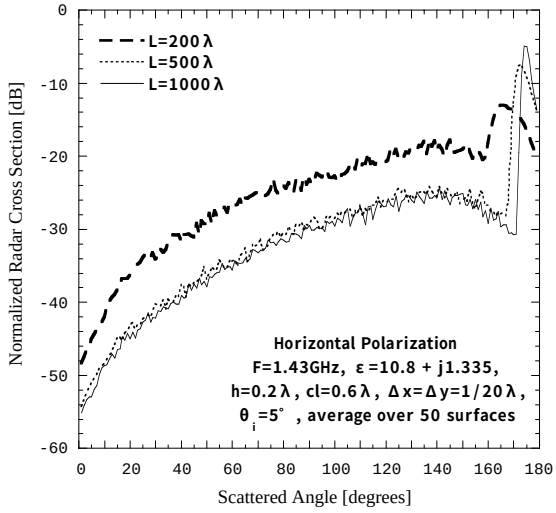

Fig. 4 Average bistatic normalized radar cross section and convergence with respect to surface length.

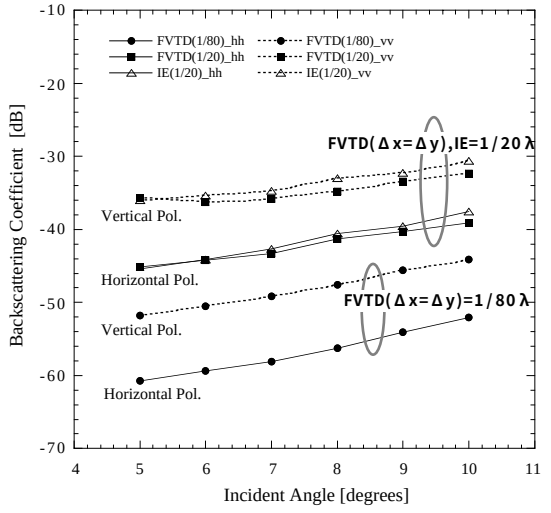

Fig. 5 Comparison of the variation of backscattering coefficients between FVTD and IE analysis at low-grazing angles.

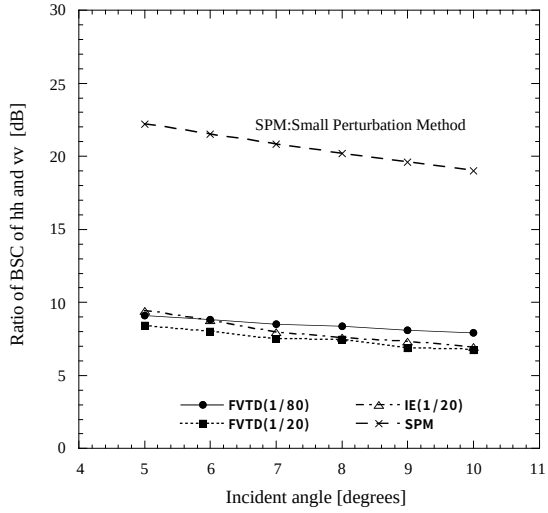

Fig. 6 Ratio of backscattering coefficient between vertical and horizontal polarizations.